



Journal of Applied and Computational Mechanics



Research Paper

Numerical Optimization of Battery Heat Management of Electric Vehicles

Szabolcs Kocsis Szürke¹, Gábor Kovács¹, Mykola Sysyn², Jianxing Liu³, Szabolcs Fischer¹

¹ Central Campus Győr, Széchenyi István University, 9026 Győr, Hungary
Email: kocsis.szabolcs@ga.sze.hu (S.K.S.); gabor.kovacs.oe@gmail.com (G.K.); fischersz@sze.hu (S.F.)

² Department of Planning and Design of Railway Infrastructure, Institute of Railway Systems and Public Transport, Technical University of Dresden, 01069 Dresden, Germany, Email: mykola.sysyn@tu-dresden.de

³ School of Civil Engineering, Southwest Jiaotong University, Chengdu 610031, China, Email: jianxingliu@my.swjtu.edu.cn

Received May 10 2023; Revised June 14 2023; Accepted for publication June 15 2023.

Corresponding author: S. Fischer (fischersz@sze.hu)

© 2023 Published by Shahid Chamran University of Ahvaz

Abstract. Lithium-ion battery technology in the modern automotive industry utilizes highly temperature-sensitive batteries. Here, air cooling strategies will be the most applicable for the chosen example based on strategies for temperature control. Simulations have been utilized to evaluate the different thermal management strategies. A battery model was developed using the solutions offered by Computational Fluid Dynamics (CFD) simulation technology. It utilizes the heat produced by the discharge of the battery cells. Due to the simulation's limited computational capacity, the energy transfer model was implemented with a simplified but sufficiently complex physical mesh. Ten actual measurements were conducted in the laboratory to investigate the heating of the cell during the charging and discharging of 18650-type batteries. The results were applied to validate the simulation model. The simulation outcomes and thermal camera readings were compared. The cell-level numerical model was then extended to examine the temperature variation at the system level. The primary design objective is to achieve the highest energy density possible, which necessitates that the cells be constructed as closely as possible; however, increasing the distance between the cells can provide superior cooling from a thermal management perspective. The effect of varying the distance between individual cells on the system's heating was analyzed. Greater distance resulted in a more efficient heat transfer. It was also discovered that, in some instances, a small distance between cells produces inferior results compared to when constructed adjacently. A critical distance range has been established based on these simulations, which facilitates the placement of the cells.

Keywords: Lithium-ion battery, thermal management, CFD simulation, battery test, thermal modeling.

1. Introduction

The recent growth in the market for passenger and commercial vehicles has led to a significant increase in the carbon dioxide emitted by internal combustion vehicles [1]. Furthermore, the demand for alternative energies and energy carriers is gradually increasing to reduce CO₂ emissions, even in transportation [2–5]. Energy efficiency has also caught up with many segments of the convergence process. Companies and researchers strive to achieve the highest possible energy efficiency in almost all areas, typically using electric energy [2–7]. As a result, green energy equipment has become an increasingly profitable European investment. The battery market is one of the fastest-growing and expanding alternative energy carriers [8]. Its many positive features make this technology a realistic alternative to fossil fuel vehicles and could play an important role in household energy supply or storage. It could also be used for long-term energy storage, even at the industrial level. The high energy density and slow self-discharge offered by some new types of batteries allow long-term energy storage on an economic scale [9]. However, the high concentration of energy stored in them carries risks. The delicate electrochemical process that allows energy use can quickly become irreversible, leading to catastrophic outcomes. Careful design and safety for users are, therefore, key factors. However, with due care, the process can be well managed and the risks eliminated.

The main problem with lithium-ion batteries is that during charging/discharging, the battery generates much heat, which causes the battery temperature to rise, especially at higher operating currents. The battery pack used in electric vehicles consists of battery modules. Each module comprises many cells/batteries connected in series and parallel, placed in a confined space. Due to the internal resistance and electrochemical reactions within the cells, heat generated at high discharge rates cannot be immediately dissipated to the environment and accumulates in the modules, leading to an increase in battery temperature and thermal instability within the module. The same is the case at high charging rates. If the battery temperature rises, the rate of battery degradation increases exponentially, and battery life is reduced, which can lead to thermal runaway [10].



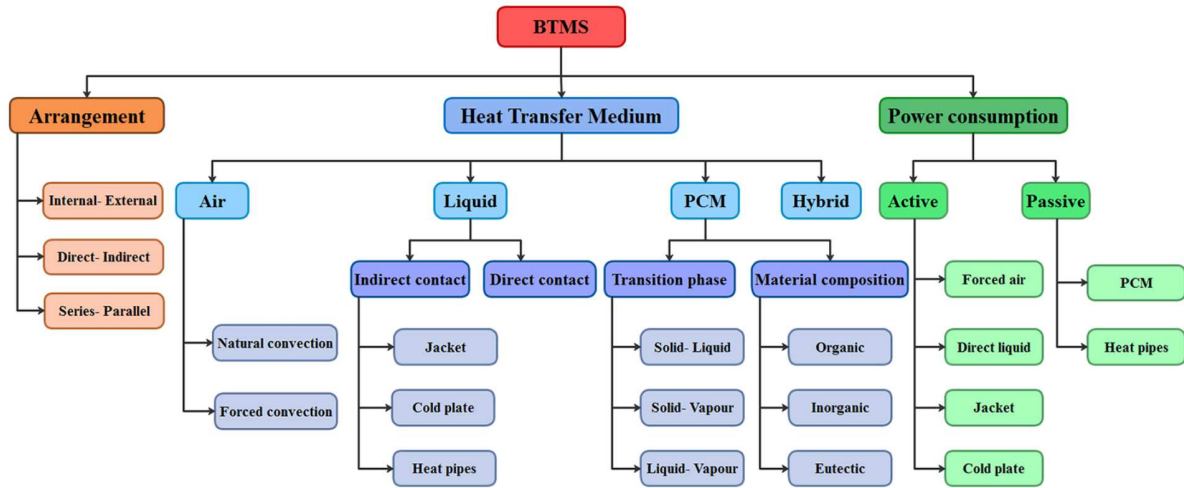


Fig. 1. Different BTMS strategies (on the basis of [14]).

The operating temperature should generally be controlled between 20 °C and 40 °C to ensure performance and cycle life. Cycle life decreases slowly below 10 °C due to anode coating and above 60 °C due to the degradation of the electrode materials [11]. (Thus, 60 °C is usually the maximum guaranteed operating temperature in the manufacturers' instructions.) However, the temperature distribution must be even to guarantee battery performance and lifetime. Therefore, the temperature distribution is controlled within 5 °C to ensure battery safety and lifetime. An uneven temperature distribution within a cell leads to varying rates of electrochemical reactions in different cell zones, resulting in partial energy consumption and reduced battery life. Studies have observed that a temperature difference of more than 5 °C within a battery pack increases thermal aging by 25% and lowers power capacity by 10%. At the pack level, seeing differences in capacity, voltage, and internal resistance between cells is typical and expected. These differences result in different thermal behavior and, thus, thermal gradients within the battery pack. A temperature difference of 5°C can cause a 1.5-2.0% reduction in battery pack capacity and a 10% reduction in performance [11, 12].

Various internal cooling techniques have been developed to mitigate the thermal problems of battery packs used in electric vehicles, such as electrolyte modification (higher tolerances), optimal electrode design, etc. In addition to the optimal design of the electrodes inside the cell, a thermal management system outside the battery pack is also needed to minimize heat generation to prevent a rapid temperature rise of the cell by proper dissipation of heat generated during charging and discharging processes. Therefore, the battery thermal management system is essential to address the abovementioned problems. Addressing the thermal problems was a key consideration in developing the BTMS (Battery Thermal Management System) [12]. Several thermal management strategies are followed in Li-ion batteries to maintain optimum temperatures and overcome the adverse effects of battery degradation, thermal runaway, and poor performance due to sub-zero temperatures. The most common classification of thermal management strategies for Li-ion batteries is detailed in Fig. 1. Thermal management systems (TMS) are typically classified based on power consumption, layout, and the medium used. A TMS can be classified as active or passive based on energy consumption.

In a passive system, heat dissipation relies solely on natural convection, whereas an active system requires energy input [13]. In addition, based on the arrangement used to circulate the working fluid, heat treatment systems can be categorized as series-parallel and direct-indirect. The parallel arrangement of the working fluid circulation is more effective in minimizing battery temperature than the series arrangement [11, 14]. In the parallel structure, since the coolant flows through all cells simultaneously, the temperature remains uniform in the different cells of the battery pack. However, it can only be achieved by ensuring a uniform distribution of the working fluid and a constant pressure differential between the inlet and outlet channels, which makes the parallel arrangement somewhat complicated. In a direct cooling system, the battery is flooded with dielectric fluid.

In contrast, the liquid is isolated from the battery in an indirect cooling system using cooling plates, jackets, or tubes. External TMS for Li-ion batteries can be categorized by the medium used, i.e., air, liquid, PCM (Phase Change Material), and hybrid. Most of the world's leading electric vehicle models fall into this thermal management group. These vehicle types all use active systems, mainly fluid-based indirect systems. These systems, therefore, dominate the current market. However, significant developments are underway to exploit the potential of PCM-based technologies. Moreover, this type of thermal management system is expected to become increasingly popular [12].

The advantages of air-cooled thermal management are that they are lighter, simpler to design, lower cost, and require less maintenance. In this thermal management system, the air is used not only for cooling but also for heating and ventilation, which again is a factor in favor of its ease of application. The air can be circulated in two ways in these heat management systems. On the one hand, forced or natural convection can be used. The latter has a lower efficiency but does not require additional energy, so the design is simpler, and the mass is lower. Forced convection is necessary when the system requires more intensive cooling. The energy can come from the differential pressure exerted by the driving wind, or electric fans can produce forced convection in a stationary position. In this case, fans accelerate the air volume for heat extraction [14]. Due to the low heat transfer coefficient of air and the increased demands of modern electric vehicles, air-based cooling cannot handle the high temperatures that can develop in the battery pack. Previous publications have shown that an air-cooled system requires about twice as much energy as a liquid-cooled system to achieve the same cooling effect. Air-cooled thermal management has difficulty cooling batteries below 50°C when battery temperatures rise above 66 °C [15]. Air cooling was predominantly used in earlier battery vehicles, but with the addition of car systems that increase the battery pack's power requirements, alternative methods can now ensure optimal operation. With the increasing electrical performance, liquid cooling technologies will be essential for the proper thermal management of the battery pack. Liquids have a higher thermal conductivity and heat capacity compared to air, which allows for an increase in the heat dissipation performance. Favorable thermal conditions allow for smaller, more compact battery pack designs. It further increases the energy density per volume, making it the most common application in the automotive industry [13, 16, 17]. However, in addition



to its excellent cooling performance, the disadvantage of liquid-based TMS is heating. Due to the high heat capacity of the fluids, as mentioned earlier, heating the fluid circuit is slow and costly. It is difficult to reconcile with the user's need for an immediate cold start on a cold winter day. Thus, using liquid-based systems for vehicle preheating is not very popular.

Although fluid-based TMS can help achieve better performance, the system's complexity and added weight will affect the vehicle's overall performance. Furthermore, the pump and liquid circuit increases the potential for breakdowns and service costs. Further simplification of thermal management while maintaining good performance is possible with alternative solutions such as using phase change materials [18]. The PCM can store and release large amounts of heat by using the energy required for phase change. The cooling process uses the material's phase change from solid to liquid to maintain the battery temperature. In research, PCM-based TMS outperformed conventional systems, and many research efforts are underway to improve their efficiency and practical implementation. A number of PCMs have been analyzed for balancing the thermal load of vehicles, including organic, inorganic, and solid-solid phase change materials. Extending the boundaries beyond which active heating/cooling is required is an appealing feature of their implementation [14,18]. In addition, PCM, Heat Pipe (HP) based cooling can partially or entirely eliminate the need for active components. It reduces the possibility of failure, overall weight, and system complexity. Compared to liquid cooling solutions, PCM-HP systems have a simpler architecture. However, they increase the system's mass, so although they take up little space in the vehicle, they are not always ideal for all applications. They are best suited for handling extreme or very high temperatures. In a well-optimized electrical system where high discharge power is not required, PCM or HP-based TMS should be considered.

Several concepts can be set up by BTMS systems to keep battery packs at the right temperature. Each technique has its advantages and disadvantages. Combinations of methods allow extreme cases to be handled with confidence. There is no universal solution. The most appropriate TMS for the desired performance and the intended operating conditions must be designed for each battery. Air cooling options are the most obvious solution for batteries intended for low-power or simple applications [14]. This strategy is the most appropriate for the battery capacity and design set as the research objective, as simplicity, ease of installation, and design are the goals. The numerical simulation approach is one of the most cost-effective methods for designing a battery thermal management system, where the optimization can be accelerated [19]. Figure 2 illustrates the workflow diagram for product development with simulation [19].

The three main input parameters are on the left side of the design process, shown in Fig. 2. The design concept, technical requirements, and models. (Physical, Chemical, and other Empirical Models) Next, CAE (Computer-aided engineering) refers to the other computational design, virtual prototype manufacturing tools used. The design problem description gives control and focuses on the investigation. Furthermore, at the end of the process, the behavioral model of the actual system and the numerical results from the specified boundary conditions are obtained.

The pilot phase and trial run consume a significant portion of the manufacturing cost of a new product. These require material, machining, the provision of the necessary boundary conditions for the trial run, and experimental equipment. In addition, prototyping and trial runs require skilled personnel, and these costs are only recovered in the case of large quantities and high product prices. This cost is significantly reduced by the use of simulation models [19]. To build a thermal model of the battery, a better understanding of the physics-based electrochemical process and the appropriate choice of governing equations, such as the energy equation, the internal heat evolution equation, and the boundary conditions, are essential in model development. In this way, the physics-based electrochemical battery thermal model estimates the internal heat generation and temperature distribution caused by the chemical reactions that occur during the charging and discharging of the battery [14]. CFD has proven to be more efficient in designing and optimizing BTMS for LI-ion batteries, as it considers the three-dimensional nature of the coolant flow and the spatial variations in heat generation around the cells. In addition, CFD also can simulate conjugate heat transfer methods, which is one of the main modes of heat transfer in the battery thermal management system [13,20].

With CFD software, it is possible to build complex physical models and solve them quickly and accurately. For example, for battery simulations, the following physical models are mentioned [20,21]:

1. Fluid Dynamics: Various cooling fluids, such as air and water, dissipate heat from a heated battery. Fluid mechanics plays a role in understanding laminar or turbulent flow.
2. Electrochemistry: The electrical part (voltage, current, resistance, and capacitance) is involved in the battery. In batteries, electrodes (anode and cathode) containing different chemicals are used for charging and discharging. Therefore, chemical reactions take place continuously during the process.
3. Heat transfer (Heat and mass transfer): thermal energy is generated in the irreversible entropy formation of the battery by the following process: Ohmic heat, Electrochemical heat.
4. Chemical reactions: Reactions like combustion are considered the Arrhenius equation to find the temperature dependence of the reaction rate—the relationship between electrochemistry and thermal energy.

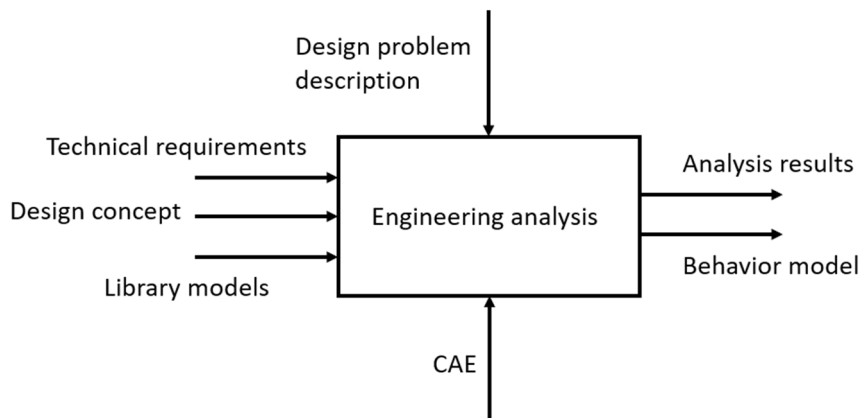


Fig. 2. Diagram of the Simulation Product Development Workflow (on the basis of [19]).



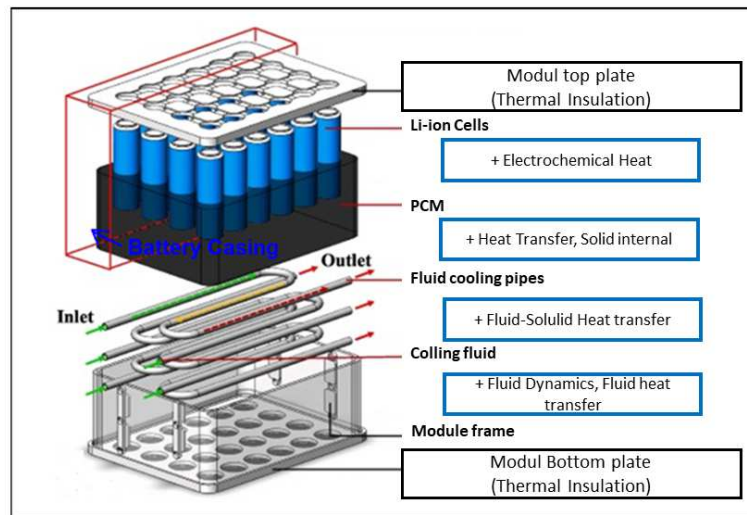


Fig. 3. Applied physics during the operation of a battery module [20].

Figure 3 shows the structure of a typical Li-ion battery module [20]. It shows that the system is complex, with several cells, including the liquid cooling circuit for cooling, whose heat transfer properties are further enhanced by the PCM layer. Also visible is the also-top tray, which defines the module's frame, with the frame enclosing it. Each unit has different material properties and physical boundary conditions (media flow or heat flow and chemical reactions). This results in the complex physics structure required for the battery module's numerical simulation, making CFD simulation modeling indispensable. It can be observed that there is a need for fluid dynamics, electrochemical models, and the use of a wide range of heat transfer models.

The current article deals with temperature-sensitive Li-ion batteries and their CFD simulation. Based on temperature control measures, air cooling strategies will be the most relevant for the chosen case. Simulations were used to assess the various thermal management solutions. A battery model was created using the solutions provided by CFD simulation technology. It uses the heat generated by the discharge of the battery cells. Due to the simulation's restricted processing power, the energy transfer model was built with a simplified but adequately complex physical mesh. Ten laboratory measurements were taken to study the heating of the cell during the charging and discharging of 18650-type batteries. The findings were used to validate the simulation model. The results of the simulation and the thermal camera readings were compared. The numerical model at the cell level was subsequently expanded to investigate temperature fluctuation at the system level. The major design goal is to attain the highest possible energy density, which mandates that the cells be built as close together as possible; however, increasing the space between the cells can provide greater cooling from a thermal management standpoint. The effect of altering the distance between individual cells on the heating of the system was investigated. Heat transfer was more efficient when the distance was greater. It was also revealed that, in some cases, a modest gap between cells yields inferior outcomes when built adjacently. Based on these simulations, a crucial distance range has been defined, making cell placement easier.

The structure of the paper is the following: Section 2 contains "Materials and Methods", Section 3 is "Investigation of the thermal development of the battery module", and Section 4 is about "Conclusions".

2. Materials and Methods

2.1. Method development and input parameters

Ansys Fluent commercial software was chosen for the numerical method development. The following will consider the hardware requirements for the simulations; hence, no above-average computer performance is available, which will be the numerical experiment bottleneck. However, the specific solutions offered by Ansys Fluent allow high performance to be achieved within a tight hardware framework. Furthermore, the user interface it offers speeds up the process as much as possible. Within the framework of the research, it was possible to test several different simulation software (Ansys Fluent, Siemens Star CCM+, OpenFoam) and to run benchmark tests with them. The carried-out simulations showed that Ansys Fluent is the most suitable software for the planned simulations. In addition, the robust mesh settings offered by the program and the use of shell regions favorable for modeling the thermal examples were significant advantages; see later for details.

The numerical solutions used may vary from software to software, and the application of some physical models may differ, but overall, the results are similar [22, 23]. Thus, only the physics the chosen software uses will be described in detail in the following. The first step in setting up the battery simulation was to study the energy equation and the models it solves. The energy transport equation of the chosen simulation solver (see Eq. (1)):

$$\frac{\partial(\rho E)}{\partial t} + \nabla[V(\rho E + p)] = \nabla \left[K_{eff} \nabla T - \sum_j h_j J_j + \tau_{eff} V \right] + S_h \quad (1)$$

where the first formula of the equation describes the relation of the flow to time (Steady or Unsteady), the second formula expresses the energy carried by convection processes. The first three terms on the right-hand side of the equation represent the energy transfer due to conduction, species diffusion, and viscous dissipation. S_h includes the heat of chemical reaction and any other volumetric heat sources that are manually defined [24]. Moreover, K_{eff} is the effective conductivity ($k+k_t$, where k_t is the turbulent thermal conductivity, defined according to the turbulence model being used), and J_j is the diffusion flux of species j . The first three terms on the right-hand side of Eq. (1) represent energy transfer due to conduction, species diffusion, and viscous dissipation, respectively. S_h includes the heat of chemical reaction and any other volumetric heat sources that have been defined [24].



To build a realistic battery thermal model, it is essential to accurately calculate the thermal energy generated by the battery, the energy flux of solid components within the material, the heat transfer between the contact surfaces of the components, the thermal energy flux between solid bodies and gases, and the transmitted thermal energy emitted by electromagnetic waves. So, the following heat conduction models are therefore needed [21]:

1. conduction,
2. convection,
3. radiation,
4. electrochemical heat.

The Energy Transport equation presented contains all of these. However, there is not enough computational capacity to solve a detailed 3D Li-ion Battery model to perform the targeted tests. Therefore, the aim is to use a simplified energy model based on an easy-to-use and apply conjugate heat transfer to achieve the goal. Therefore, some models will not be solved.

Of the four main models, the implementation of the first two heat transfer models in the simulation model is essential. The combined effect of several components will prevail. Medium flow is assumed both within the designed module and between the cells. It is planned to exploit natural convection's potential and even uses forced convection-enhanced heat removal. For this reason, convective thermal models are also indispensable. However, the scale of radiative heat flux is small compared to the first two. However, its application in a simulation environment would drastically increase the complexity of the model and, thus, the simulation costs. Therefore, the Radiation is omitted in the model built.

The application of an electrochemical thermal model is not necessary (or even appropriate) for the problem to be studied. The desired results do not require a model of the electrochemical process. Only the amount of heat generated by the process is required, which can be defined in terms of the volume of the elements. Practical measurements or analytical solutions can determine the exact value of the heat quantity based on knowledge of material properties and electronic boundary conditions. This paper uses and verifies the theoretical solution with physical testing. Thus, the main focus is on the accurate determination of the Conduction and Convection model and boundary conditions.

2.1.1. Conduction

Regarding the thermal conductivity within the material, several assumptions have to be made, which also lead to deviations from the real physics but are unavoidable for the practical applicability of the model. These properties are mainly material property conditions. First, the amount of heat produced by the battery's electrochemical reaction will be defined as a volumetric heat source. Then, to calculate the energy flow accurately, the density of the material, its specific heat capacity, and its thermal conductivity are needed. The software calculates the energy equation over solid regions using Eq. (2):

$$\frac{\partial(\rho h)}{\partial t} + \nabla \cdot (\nu \rho h) = \nabla \cdot (k \nabla T) + S_h \quad (2)$$

where ρ is the density, h is the sensible enthalpy, k is the conductivity, T is the temperature, and at the end, S_h is the volumetric heat source [24]. These properties can change over time and with changes in certain boundary conditions in a real thermodynamic process. It must be taken into account that some materials and material properties have variable thermal properties that can change with environmental changes, such as an increase in temperature. The simulation software can define these. It is possible to define certain material properties for the model by means of dependencies, even by means of a graph based on empirical experience, instead of constant values. However, defining material properties, in this way, is associated with an increased computational effort [24]. Therefore, several assumptions are made here further to simplify the calculation of the battery temperature field. Each material has the same thermal conductivity in one direction. The temperature gradient does not affect each material's specific heat and thermal conductivity. During charge/discharge, the current density and the heat generation rate are uniform.

2.1.2. Convection

Natural convection is when the movement of a fluid in a liquid is caused by the difference in density (buoyancy) caused by temperature gradients [24]. This physical phenomenon must be taken into account. Convective flow can be expected to occur in air layers of varying volumes found between cells with rising temperatures. Thus, the fluid dynamics trajectory must be built up in the simulation model with sufficient accuracy to model convective flows accurately. Among the fundamental conditions of fluid dynamics, the determination of pressure, density, viscosity, temperature, and gravitational acceleration are essential. When the gravitational acceleration is added, the equation of momentum will be as follows (Eq. (3)) [24]. The gravitational acceleration is defined as 9.81 m/s^2 in the Z coordinate. The momentum equation in the Z direction is shown in Eq. (3).

$$\frac{\partial(\rho W)}{\partial t} + \nabla \cdot (\rho U W) = \mu \nabla^2 W - \frac{\partial P'}{\partial z} + (\rho - \rho_0)g \quad (3)$$

A crucial definition of pressure is that an incompressible-ideal gas model is used to model the air region. Thus, the air density is a function of the set base pressure of the process as follows [24]. The ideal incompressible gas model is used when pressure changes are small but temperature changes are significant. The incompressible-ideal gas option for density treats the density of the fluid as a function of temperature only. If the above condition is satisfied, the incompressible ideal gas law generally provides better convergence to the ideal gas law without sacrificing accuracy [25]; see Eq. (4):

$$\rho_0 = \left(\frac{P_{op} M}{RT} \right)_{average} \quad (4)$$

where a P_{op} is the ambient pressure (Operation conditions), M is the molecular Weight, and R is the universal gas constant.

2.1.3. Battery Cell Structure Build-up

The simulation software had to build a model of the battery cell. Knowing the possibilities offered by the software and the cell type, it is possible to perform accurate simulations. The chosen battery cell is the 18650-standard type. It consists of a metal casing 18 mm in diameter and 65 mm high, a coiled Jelly-roll, and positive and negative terminals welded at both ends (Fig. 4) [26]. The Jelly-roll contains the anode, cathode, and separator foils. Knowing the dimensions and material properties of the cell elements, the numerical model can be set up. However, the choice of CFD Simulation method to use for detailed geometric modeling and the



large surface area of the coiled-coil Jelly-roll meshing poses a significant challenge to the overall computational capacity. Therefore, simplifications are regularly applied when building battery thermal models regarding geometric mapping or physical settings [26–28]. In order to circumvent the physical model used, Bernardi's method was used to determine the rate of thermal expansion derived analytically. Several other studies have already used simplified models [26–29]. However, the solution detailed below also includes radical simplifications to the complexity of the physical model of the cell but also includes virtual regions (not part of the mesh) to increase accuracy. Figure 4. illustrates the structural differences between each cell model solution.

The first example in Fig. 4 shows the construction of a standard 18650 cell. It is followed by a simplified structure model, whereby the components of the Jelly-roll have been merged and applied as one large solid battery. In this case, of course, the thermal properties specific to each element must be brought into the common denominator to get a relevant picture. Around the merged cell core, there is still the physical form of the insulating PVC film, the cell box or can, and the geometry of the positive and negative terminals. In itself is a significant simplification. At the simulation scale, however, testing the resulting models at the module level is still critical to implement in the absence of more serious workstation computers. A completely simplified cell core model with merged material properties was defined as a solution. The external components, the cell can, the PVC foil, and the definition of the Terminals in physical form, so in the finite element meshes, are not represented. Taking advantage of the CFD simulation, these models will only be visible in virtual form as 1D-model for the energy equations, using the so-called Shell conductions (Fig. 4. Simplified Cell Core Model).

The use of Shell regions allows the elimination of the need to model and mesh individual components physically, thus reducing preparation energy, avoiding increased meshing and solution time, and preparation tests have demonstrated order-of-magnitude memory savings (see later) [28, 29]. Having a coherent mesh of interfaces is very important in terms of meshing. For these interfaces, Solid-Fluid interfaces, a strictly conformal mesh has been used. In addition, topological partitioning was already done during the preparation, so the interface design supporting heat transfer on the contact surfaces could be easily developed (Fig. 5).

As shown in Fig. 5, Shell regions are defined between the Wall and Wall-shadow interfaces created on the Solid-Fluid contact surfaces. However, the virtual regions must affect the energy transfer for accurate thermal modeling. Where appropriate, they can insulate or dissipate thermal energy from the cell core, or, in the case of terminals, they can also generate additional heat. According to Fourier's law, the authors refer to the individual layers and materials as the 1D model (Fig. 6) in these regions (Eq. (5)) [25]. Heat conduction and heat transfer through the battery walls in the thermal model can be represented as follows [29].

Since no precise information exists on the Contact Resistance between layers, its definition is omitted. It is estimated to be of negligible order of magnitude [25]. To calculate thermal resistance, see Eq. (5):

$$R = \frac{t}{k A} \tag{5}$$

where t refers to the thickness of the Shell region, k is the characteristic conductivity of the material defined by the region, and A is the surface mesh generated on the interface. The Shell regions along the cell model were defined as shown in Fig. 7. to reproduce the real battery cell operation:

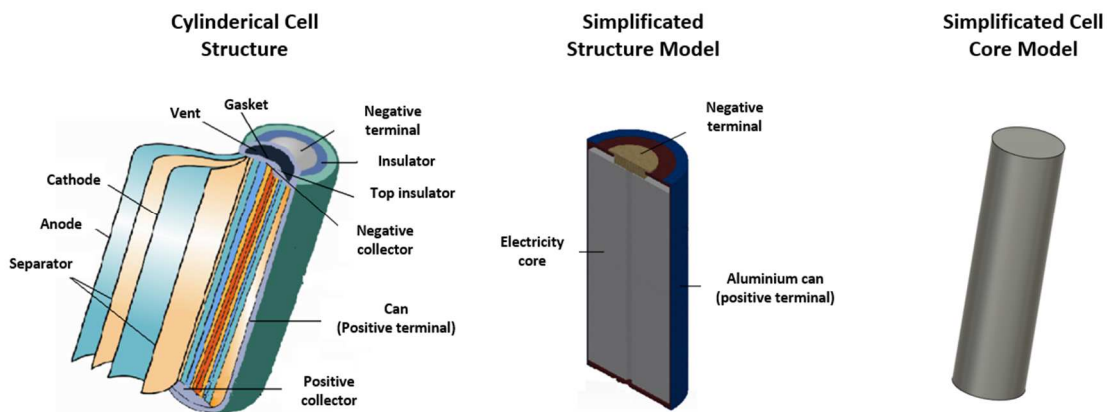


Fig. 4. Different Cell Structural models.

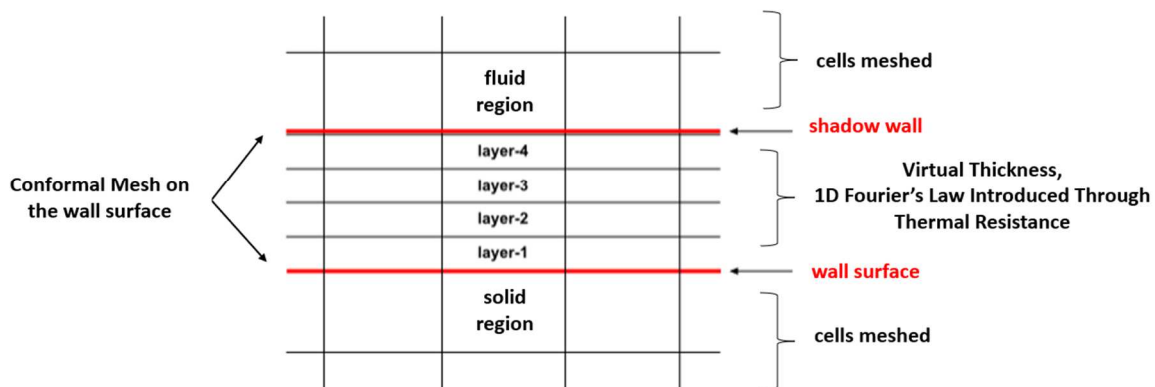


Fig. 5. Shell conductions in Ansys Fluent.



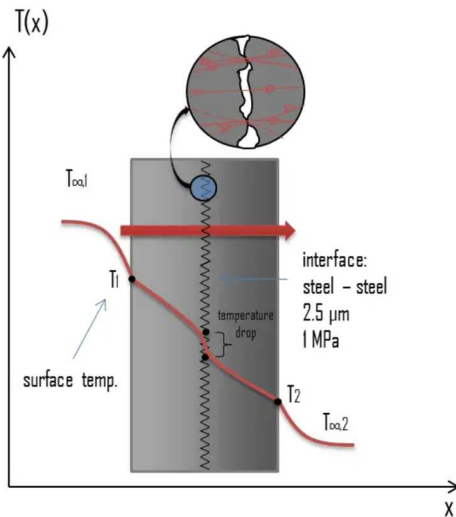


Fig. 6. Thermal Resistance through walls [29].

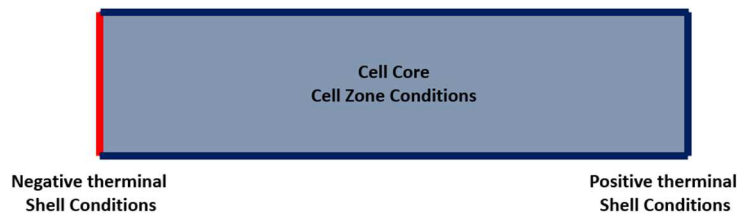


Fig. 7. Shell Conduction Properties in Ansys Fluent.

To define virtual regions correctly, it is essential to define accurate material properties and wall thicknesses. As well as an accurate derivation of the thermal properties of the solid jelly-roll. Following a previous example, the material properties and the thermal expansion rate of the 18650 batteries were used to set up the new model. The components and material properties of the 18650-battery cell are shown in Table 1 [26]. The volume-averaged material properties calculated for the simulation model are as follows (see Table 2).

Table 1. Material and thermal properties of cell components.

Component	Materials	Density [kg/m ³]	Specific Heat [J/(kg°C)]
Cathode	LiFePo4	2,300	1,300
Positive collector	Al	2,710	903
Can (positive terminal)	Al	2,710	903
Negative collector	Cu	8,930	386
Negative terminal	Steel	7,900	460
Separator	Pe	1,400	1,551
Electrolyte	(EC+DEC+EMC+DMC)	1,223	1,375
Parameter	The Positive electrode sheet	The negative electrode sheet	The separator
ϵ	0.25	0.33	0.47
δ	0.455	0.304	0.241
$\lambda m/W/(mk)$	1.48	1.04	0.351
$\lambda f/W/(mk)$	0.59	0.59	0.59
$\lambda l/W/(mk)$	1.201	0.895	0.466

Table 2. Volume averaged values to be used in the model.

Component	Material	Density [kg/m ³]	Specific Heat [J/(kg°C)]	Heat transfer rate [W/(mk)]
The cell core	Mixture of Anode/Cathode/Separator	2,000	900	X-Z direction – 1.6 Y direction – 3.0
Al Can, Positive terminal	Al	2,710	903	238
Negative terminal	Steel	7,900	460	20
Insulation film	PVC	920	1,000	0.3344



Table 3. Thermal performance calculated for the model.

Parameter name	Parameter value
Temperature	298 K
Discharge rate	1C
Electrical core	12,825 W/m ³
Positive terminal	126 W/m ³
Negative terminal	735 W/m ³

The heat generation rate of the cell core can be calculated using the Bernardi heat generation model (see Eq. (6)):

$$q = \frac{I}{V_b} \left[(U_0 - U) + T \frac{dU_0}{dT} \right] = \frac{I}{V_b} + \left[I \times R + T \frac{dU_0}{dT} \right] \tag{6}$$

where V_b is the volume of the cell, I is the charge/discharge current, T is the temperature, R is the internal impedance of the battery, and $dU_0 = dT$ is the coefficient of the open circuit voltage with temperature. The cell core heat generation values relevant to the model are given in [26] (see Table 3).

The values given in Table 3., for the main structural units of the battery cell are the thermal expansion power in W/m³ calculated from the material properties using Eq. (6) (at 25 °C, i.e., 298 K ambient temperature and 1C discharge rate.)

The battery has meshed with Polyhedral (Regular Hexagonal Cell Volumetric Cell Type) batteries. A grid independence test was carried out, which proved that the chosen type could guarantee sufficient accuracy and cell number usage for the required tests. Several different mesh types and meshing strategies were tested during the modeling. However, in preparation for the module-level simulations, some meshing solutions (use of cell volume sweep methods due to better structure design, Hexahedral, Tetra elements) caused interface and convergence problems. Nevertheless, polyhedral meshing proved to be the most stable for the full range of module-level measurements in testing. The meshing can be seen in Fig. 8.

Based on these results, a finite element model of the battery cell was created. The meshed model was not larger than 10,218 cells. It compares to the structured cell model presented previously [25], which had a mesh element count of approximately 50,000 elements per battery. It is an order of magnitude improvement, and it is now achievable to perform module-level transient simulations using an average personal computer. Using four processor cores, a 1C discharge transient simulation with 1-hour intervals took only 3 hours to run for the laptop used to run the validation experiments. Thus, even with a 4x4 module size, a reasonable run time can still be planned.

2.2. Cycle test for validation

Laboratory measurements were carried out in preparation for the simulations. The aim was to perform the laboratory measurement under the specified boundary conditions on a 18650 cell. Environmental disturbances, such as airflow or temperature variations, had to be excluded as much as possible, so the battery to be measured was placed in a closed metal box. A LabVIEW program recorded the data, while the temperature data were documented by a temperature sensor placed in the chamber and on the cell's surface. The temperature of the battery was measured using cycle tests. The measuring system's block diagram and the box utilized for the measurement are shown in Fig. 9.

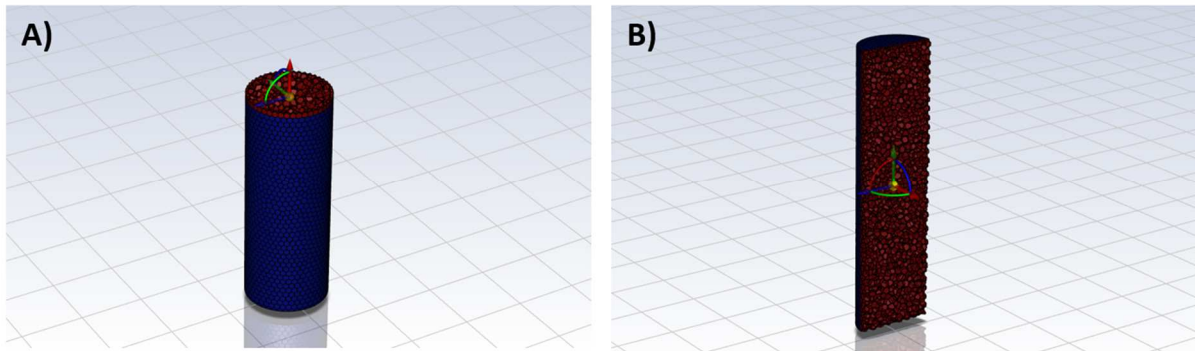
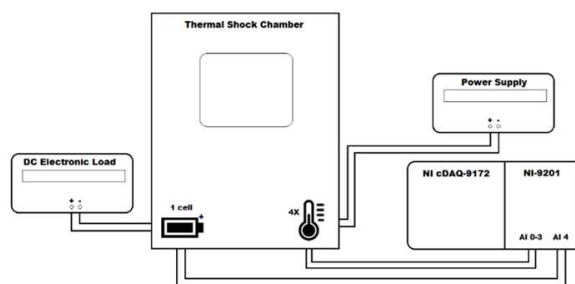


Fig. 8. (a) Cell Mesh cross-section Z; (b) Cell Mesh cross-section Y.

A) Measuring system block diagram



B) Metal box used for measurements



Fig. 9. (a) Measuring system with block diagram; (b) Metal box during measurements.



Figure 9(a) shows a block diagram of the measurement system on the left and the box used for the measurement on the right (b). The following system was used to perform the tests: power supply: Hameg HMP 4030; dummy load: Elektro-Automatik EL3160-60A; data logger: NI 9201; temperature sensors: LMT85LPG; battery type: Samsung 26F 18650; central computer for test control with LabView software package. During the measurements, four temperature sensors were used, two of which were attached to the top and bottom of the 18650 battery, one to record the temperature of the box and one to sample the temperature of the laboratory. In addition, the following structure was used to perform the cycle measurement:

- a) Charge between 0% - 100% SOC using the CC-CV method with a current of 1C (2.6 A) maximum voltage level is 4.2 V.
- b) Pause, duration: 1 h.
- c) Discharge between 100% - 0% SOC with 1C (2.6 A) current, lower threshold voltage 3 V.
- d) Pause, duration: 1 h.

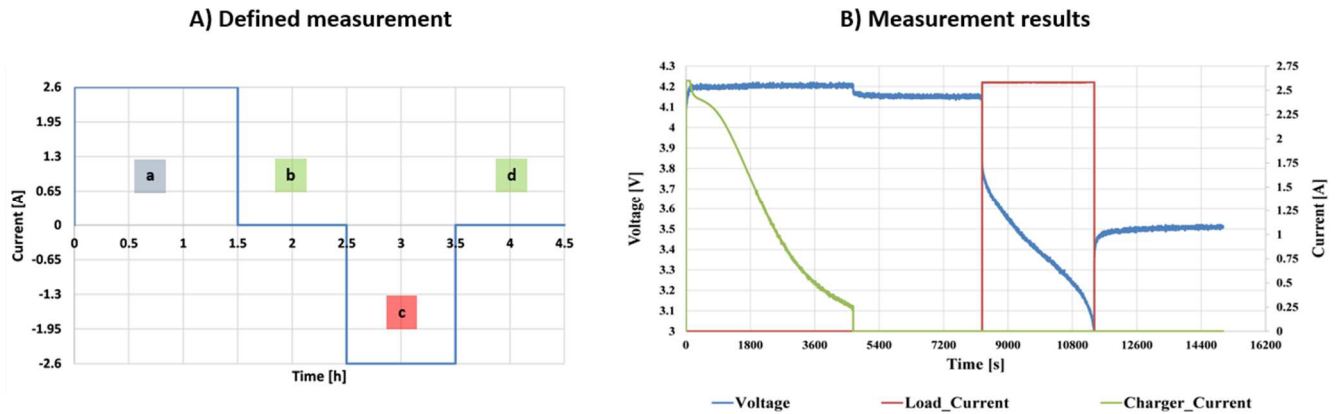


Fig. 10. (a) Cyclical measurement concept steps; (b) Capacity test result.

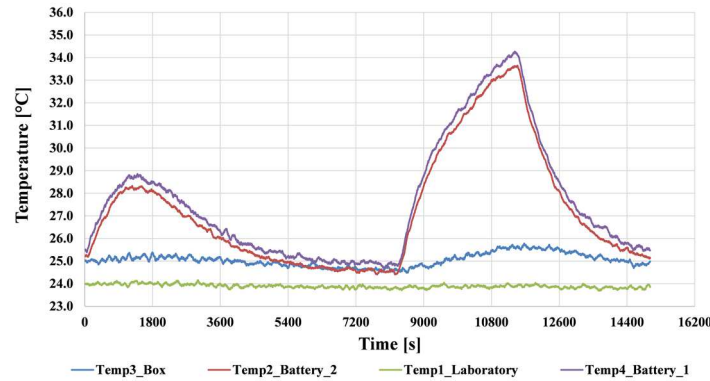


Fig. 11. The temperature change of the third measurement.

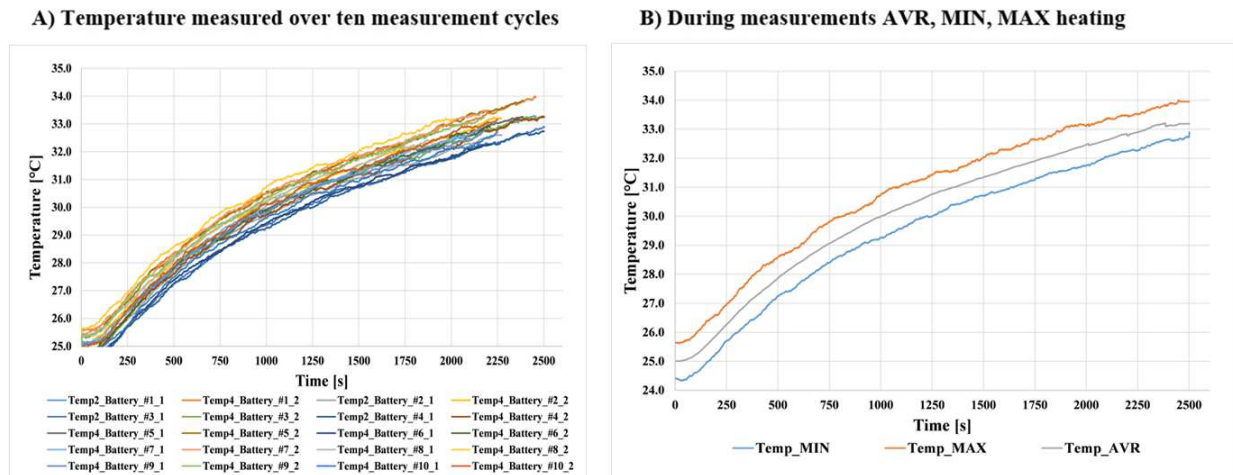


Fig. 12. (a) Data from the sensors on the batteries of the ten-cycle measurement; (b) Minimum, maximum, and average values of the measurements.



Figure 10 shows the defined measurement plan and a test result. Figure 10 also shows the draft cycle measurement plan on the left (a) and the test results on the right (b). From Part A, it can be seen that it is composed of 4 phases: charge, pause, discharge, and pause. The cyclic tests have been performed a total of ten times. The charging (green), discharging currents (red), and the voltage measured during the whole test are shown in blue on side (b) of Fig. 10. It is important to note that the Samsung 26F battery was not in brand-new condition for the tests, with an average discharged capacity of 75%. Fig. 11 shows the temperature sensor data for tests.

Figure 11 shows the data from the four temperature sensors, with the laboratory in green and the box temperature in blue. The data from the sensors on the cell are shown in purple and red. From the figure, it can be observed that there is heating even with a 1C charge and discharge. It is less during charging, mainly during the higher charging current during CC mode, and cooling is already observed during CV mode. Progressive warming was observed during discharge, with the cooling process starting only during the higher voltage and resting phase. During this type of loading and charging, significant changes occurred during discharge, and this will be analyzed in detail later. The measurement was repeated ten times in total, the results of which are shown in Fig. 12.

In Fig. 12(a), it can be observed that the nature of the heating was very similar in all measurements. From the figure, it can be observed that the difference between measurements was not greater than 1.6 °C. The average time of the tests was 2500 s due to battery degradation. Figure 12 (b) shows the difference between the measurements, with an average difference between MIN and MAX of 1.34 °C.

The battery cell and the environment corresponding to the real measurement conditions were then built in the CFD simulation software. The dimensions and wall thicknesses match, and the cell is placed in a similar position in the test environment. Figure 13 shows the battery cell in the box and the solution in the model.

It is important to note that the chamber, as the battery environment itself, also appears in the simulation model, as the chamber's temperature also increased during the measurement. Figure 14. shows the cell placed in the box in the simulation environment.

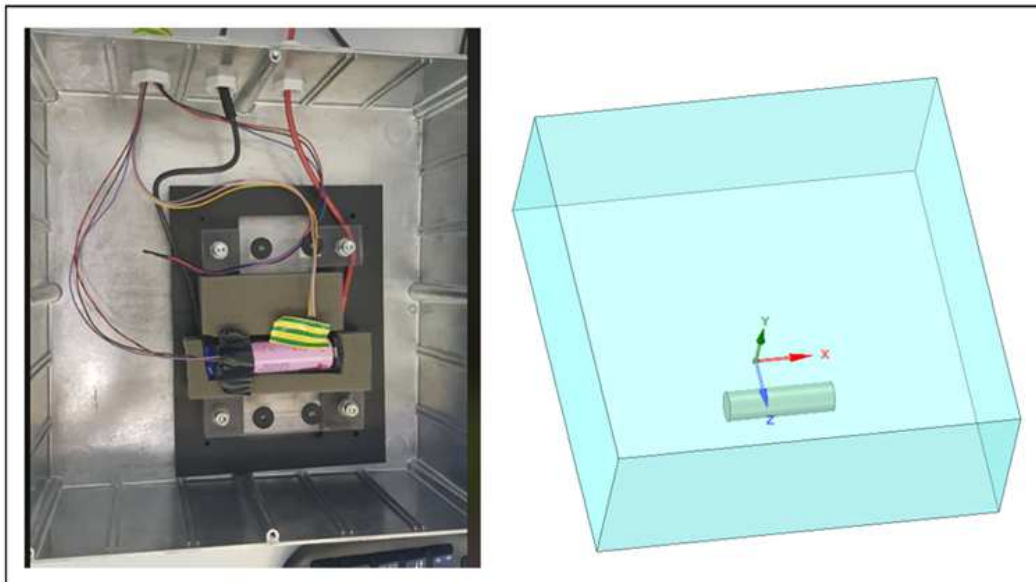


Fig. 13. The Measurement box and model side by side.

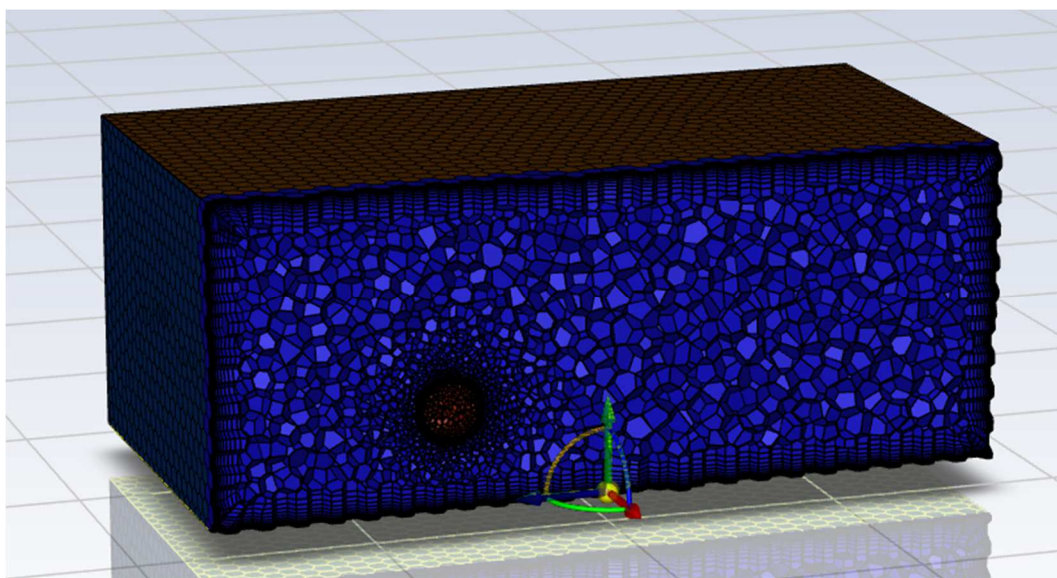


Fig. 14. The meshed cell and box model.



An ambient temperature of 25 °C and a corresponding heat dissipation factor of 10 W/m² were defined for the external walls of the chamber. The air mass modeled inside the chamber was also determined using several material properties: specific heat, density, viscosity, and pressure. For the material properties of the air, it is vital to highlight the correct definition of pressure. Using constant pressure, a difference of an order of magnitude was observed between the simulation results and the measured values. Therefore, from a fixed initial value, it was necessary to allow it to vary as a function of temperature so that the natural convection could be established under the influence of the given gravitational direction and acceleration. As a result, the ideal gas model was required [24].

2.3. Comparison of simulation and measurement results

The simulation results were aggregated with the measurement results of the ten real tests. Figure 15 shows that the initial heating of the cell coincides with the average heating curve of the ten measurements. The key difference, however, is that the simulated result describes a perfect curve, perfectly regular and continuous. Therefore, deviations are observed in the middle section. Furthermore, the minimum value of the simulated cell converges to the minimum of the measured values. It is important to note that in the simulation, the minimum values would have been measured in the opposite half of the cell due to the continuous convective flow. In the case of a real measurement, no temperature sensor was placed on the other half of the cell. Therefore, the minimum temperatures detected during the testing were probably not recorded. There is already a difference between the observed average and the simulated values in the last quarter of the graph. The slight increase in ambient temperature seen during the measurement conditions can explain this. Another critical factor is that fewer measurement data were available for this region, increasing uncertainty.

An earlier direct comparison measurement was made to validate the simulation process, where thermal camera images of the measure were taken in addition to the thermal sensors for visual comparison. In this case, the aim is to compare the direct measurement results of one cell with another of the same conditions in a simulation environment (see Fig. 16).

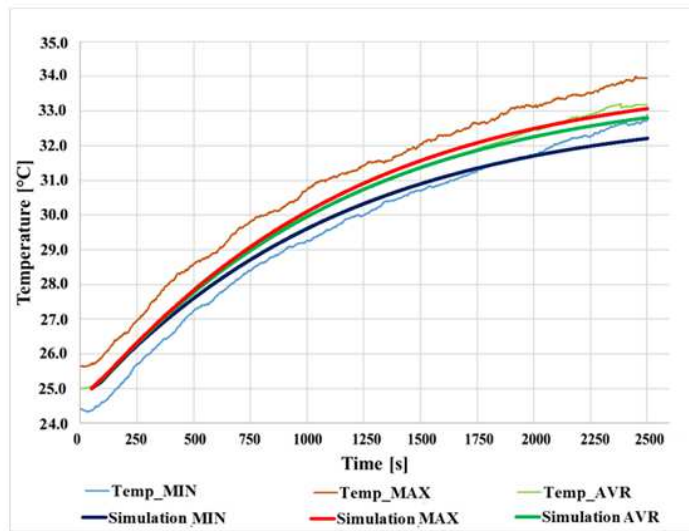


Fig. 15. Comparison of real measurement results and simulation results.

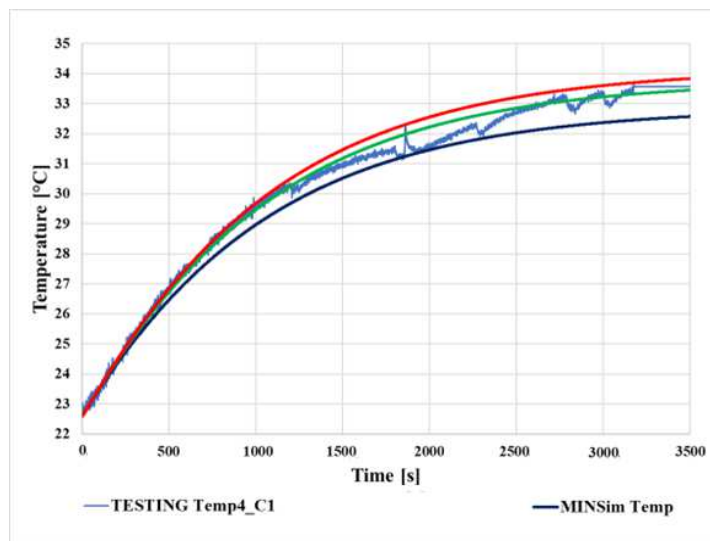


Fig. 16. Comparison of real measurement results and simulation results during the thermal camera test.



The measurement results were slightly affected because the chamber cover had to be temporarily removed to take the thermal camera images. It allowed fresh air to reach the battery, thus temporarily affecting the chamber temperature slightly. The diagram shows that the cell temperature also drops at the opening points. Then, after the thermal camera recording, it converges again to the curve that was started. In contrast, the simulation results show a temperature rise curve because they were modeled in a perfectly closed chamber. Independently, it can be concluded that the measurement results and the CFD simulation results correlate well. The average peak temperature values measured at the end of the discharge and the average values measured simultaneously in the simulation differed by less than 1%. For the visual evaluation, images captured by the thermal camera were used, and the simulation images were also taken using the same color scale setting. Figure 17 shows the image taken at 3300 s and the cell heat map taken during the simulation simultaneously in the model plane.

Figure 17 shows that the measurement and simulation images give the same temperature and temperature distribution results using the parameters defined in the previous section. Furthermore, it can be seen that the real measurement and simulation curves are also similar.

In the next section, these results have been used as a basis for the analysis at the module level.

3. Investigation of the Thermal Development of the Battery Module

The next step in the analysis is to examine the 4x4 module level. The extended analysis will use the simulation model settings partially derived in the previous section. The physical and mesh criteria are still applied to consider the results optimized by the measurement. Figure 18 shows the module used for the simulations.

Figure 18 shows the modeled battery module to investigate the heat dissipation of the cells to the environment, which is designed to examine increasing cell spacing and contains a total of 16 batteries. All boundary conditions are identical to those seen in the previous simulations, with only the module's geometry changing. The distance between the cells, as well as between the edge cells and the module walls, increased gradually. Meanwhile, the simulation was used to measure the resulting temperature profile. Each simulation, up to 3600 s, examined the heating of the module. After 3600 s, the environment and the cells had not yet reached equilibrium. However, it is unnecessary to investigate the module heating over a more extended period, as even the battery cells in the new state are discharged at constant discharge 1C.

The tests started with cells almost entirely in contact. The minimum cell spacing was 0.01 mm due to numerical instability (hence this condition is 0 mm in the following). The quality of the meshing did not allow for a satisfactory accuracy of the calculation of the cylindrical surfaces in contact in the model. The maximum distance was 12 mm, as shown on the right side of Fig. 19.

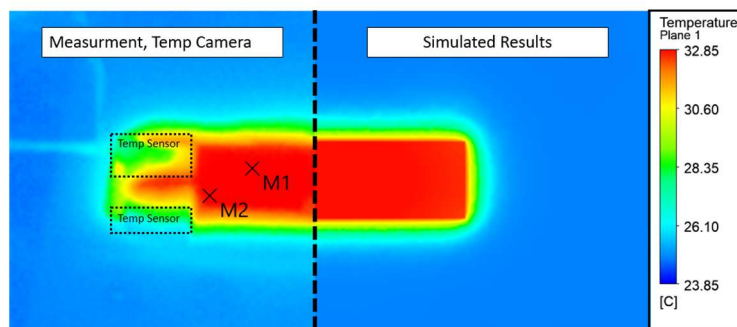


Fig. 17. Comparison of the thermal camera image and the simulation image.

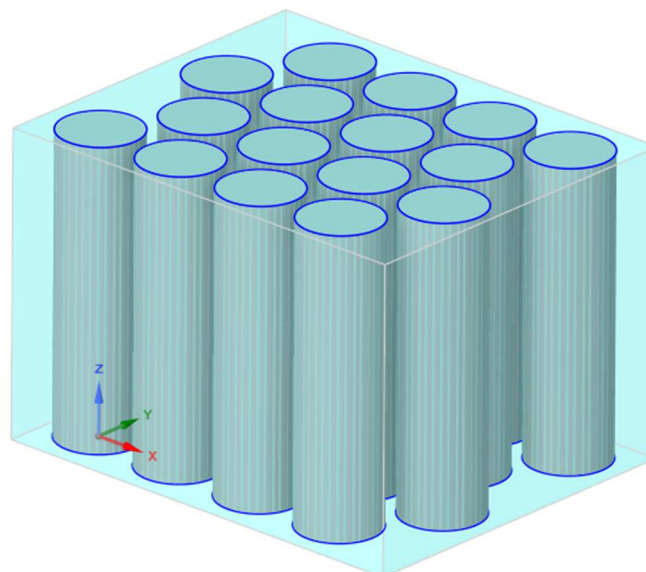


Fig. 18. Geometric model of the 4x4 module.



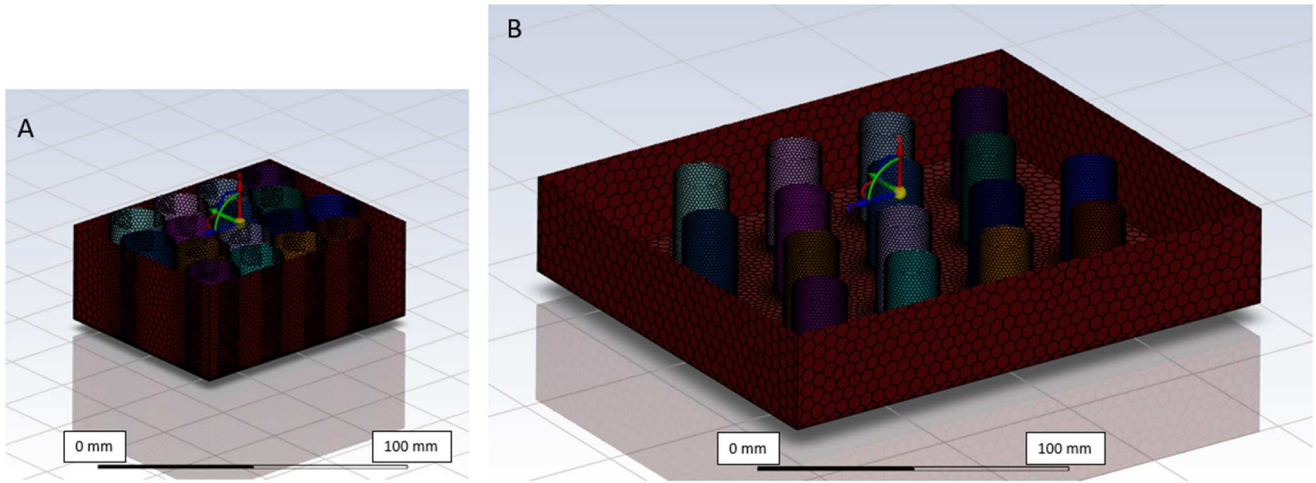


Fig. 19. Section images of the finite volume model of the module for minimum (a) and maximum (b) distance.

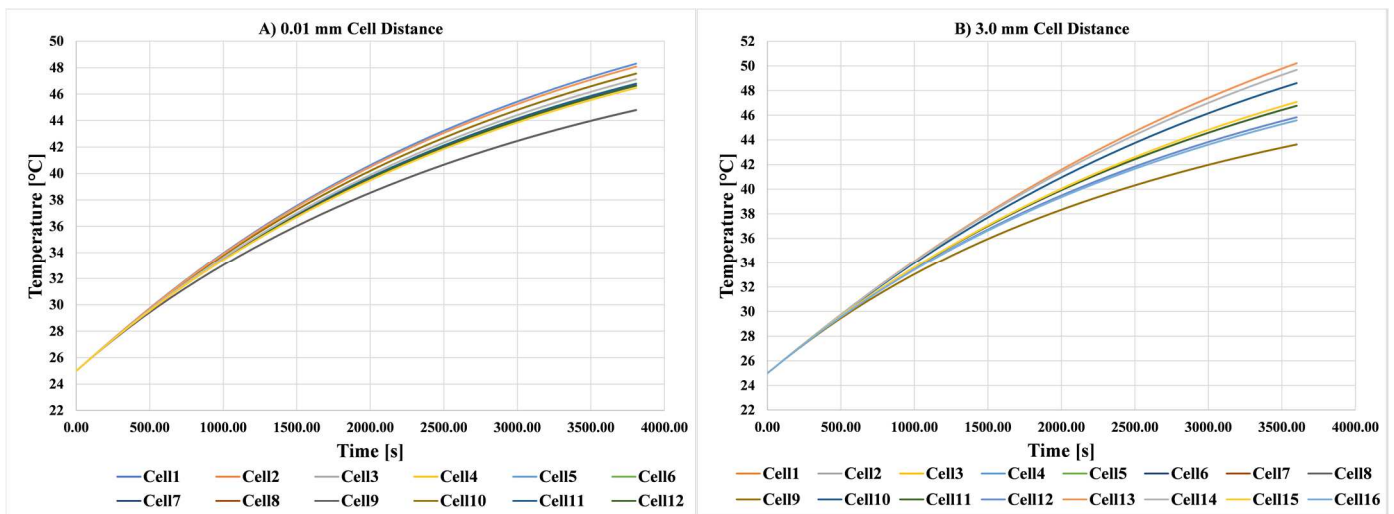


Fig. 20. (a) 0.01 mm and (b) 3 mm Cell Distance module thermal simulation results.

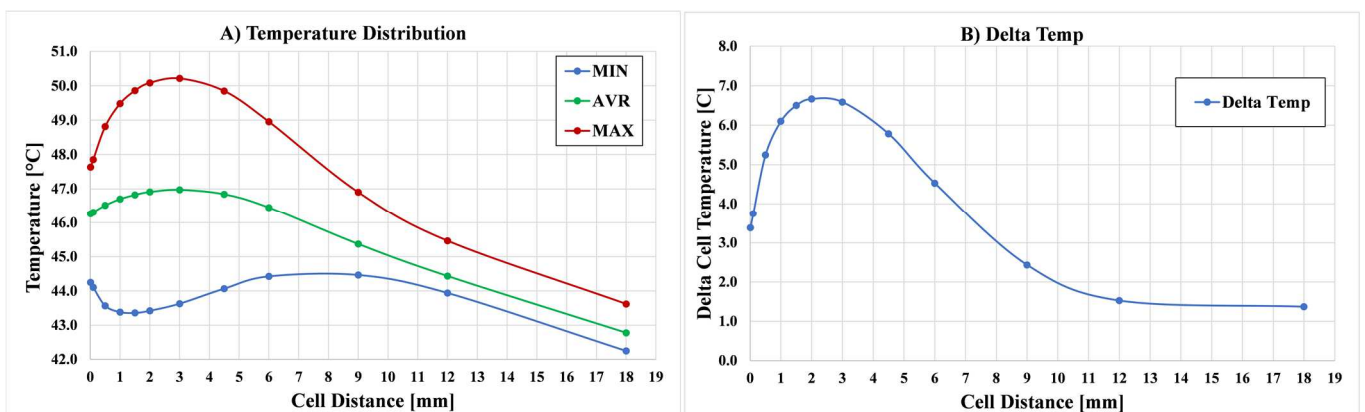


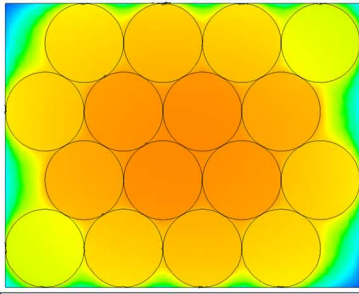
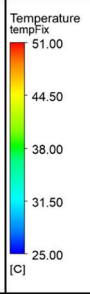
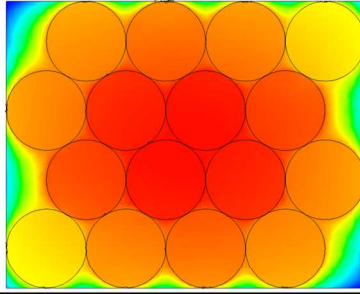
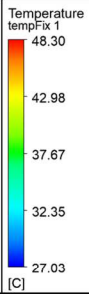
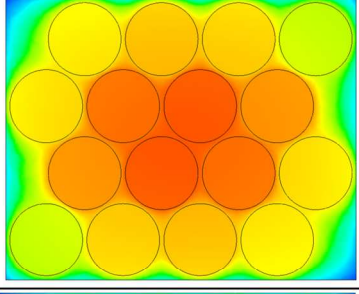
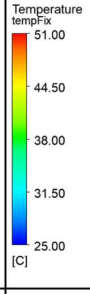
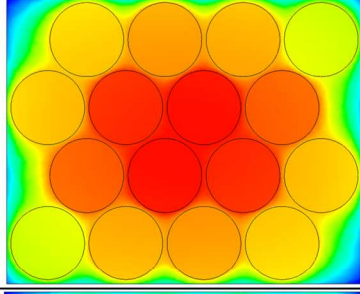
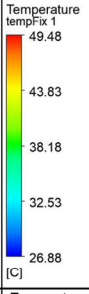
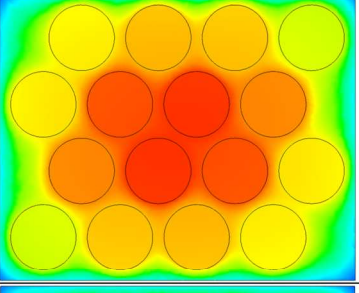
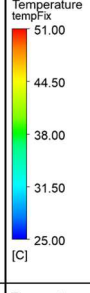
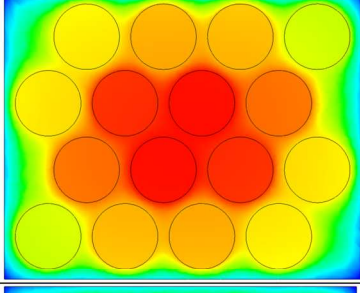
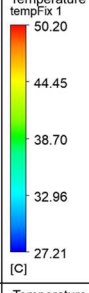
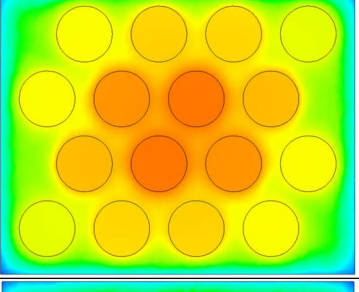
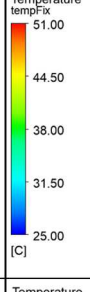
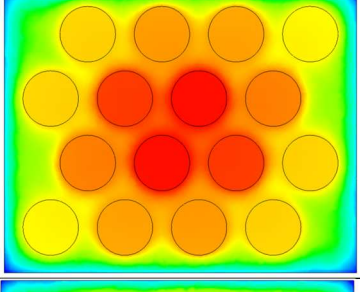
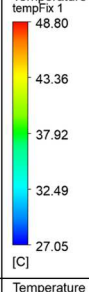
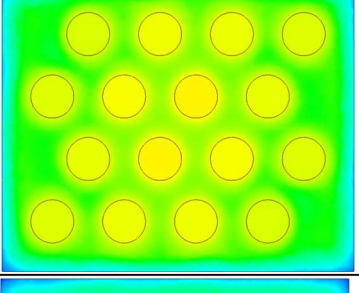
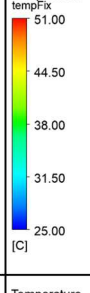
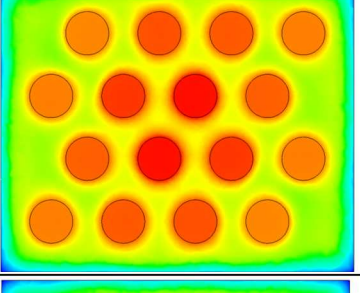
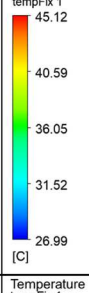
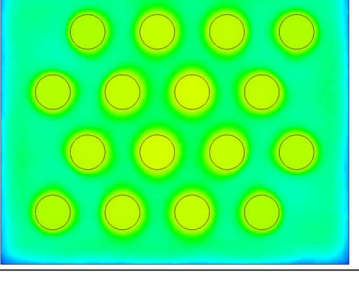
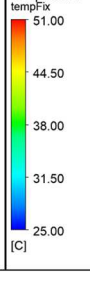
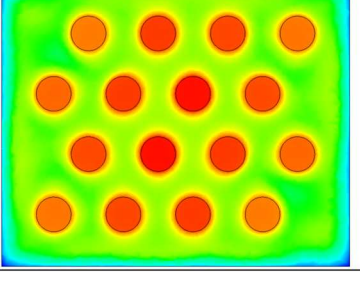
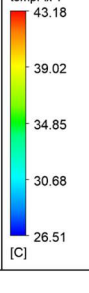
Fig. 21. (a) Min and Max Temperature distribution of the cells inside the module due to the continuously increasing air gap between the cells. (b) Delta temperature inside the module.

In this case, the heat distribution of the cells is favorable, with the temperature of the outer cells being only slightly lower than that of the cells in the middle.

Figure 20 shows the thermometry of the battery cells and the difference between the minimum and maximum temperatures inside the module. This difference is profiled at a cell-to-wall distance of 3 mm. However, if someone looks for the lowest value of the minimum temperatures measured on the cells, it is shifted to the 6 mm cell to module wall distance.



Table 4. Temperature distribution in cross-sectional images.

Cell Distance	Uniform Color Range	Legend	Local Color Range	Legend
0.01 mm				
1.00 mm				
3.00 mm				
6.00 mm				
12.00 mm				
18.00 mm				



In Fig. 21, it can be observed that the temperature level of the module started to increase gradually with increasing cell distances of 0 mm. The temperature peaks at a 3 mm wall-to-cell distance. Then, all temperature values begin to decrease again with a further increase in the distance. Finally, the system reaches a range where the cells behave as separate cells due to the distance. Considering the recommended maximum operating temperature, i.e., the maximum of 40 degrees Celsius defined earlier, the figure shows that the module is constantly overheating. With a gradual increase in spacing, temperatures decrease and start to become favorable at 18 mm spacing. However, this means that the size of the module is such that the energy density per unit volume is already unfavorable, i.e., the size of the module would limit its use. The general aim is to strive for the highest possible energy density so that the battery pack can provide the user with the most significant possible power and, where appropriate, range. For a better understanding, the cross-sectional heat map of the module produced by the simulation was analyzed. For each case, a record was made showing the volume of the cells and the module. The most relevant images captured at cell distances are now presented in Table 4.

To design the ideal module, efforts should be made to maximize energy density and maintain the ideal temperature. Using fully packed cells within a module seems to be a favorable choice. However, this does not allow a cooling system between the cells. Therefore, additional heat must be extracted through the module walls to ensure ideal operating conditions. However, if this solution were chosen, it should also be considered that larger temperature differences between cells within a module may occur. The cells in the wall will cool faster and better due to the increased heat dissipation through the module wall, while the cells inside will only be able to cool down due to the material properties of the battery and the thermal conductivity of the air trapped between them. However, in some cases, this can be uncomfortable and requires further investigation. However, if the remaining space between the cells in the module were to be filled with a material with increased thermal conductivity, it is likely to increase the overall cooling capacity of the module by an order of magnitude, and the temperature differences between the cells would be much more evened out. Higher cooling capacity should be expected if the module is built with some cell spacing, leaving room for an intercooler. However, the increased air mass inside the module further reduces the thermal conductivity of the module unit. However, a significant advantage is that there will be enough space to move the intermediate air between the cells. It can be facilitated by increasing natural convection. Higher flow rates also mean higher cooling capacity. It will also be possible to control the airflow, thus improving the temperature distribution and reducing the extremes. Fans can also enhance air circulation. In this case, it may be interesting to consider the positioning of the cells and their overlapping in terms of air path or to examine the ideal spacing as a function of the pressure drop of the flowing air.

4. Conclusions

An efficient thermal simulation model and method have been developed to investigate the heating problems of battery cells. The built model can solve simulations efficiently and reliably with minimal computational resources. It also allows the testing of many new ideas during the design phase, thus reducing manufacturing and testing costs. Ten real charging and discharging (1C case) tests were compared with simulation results to validate the model. The simulation results showed sufficient accuracy. Therefore, simulation is performed at the module level to test battery TMS.

The results show that increasing the distance between cells is not always the better cooling option. Also, a 3 mm cell spacing shows a higher heating effect. A larger space has already had a beneficial effect on system cooling during design, so it is worth considering that building the batteries completely side by side is a better solution in some cases. However, for applications that require more cooling (higher load), it is worth considering the heating correlations determined from simulations. In the future, the module-level simulation results can be refined and improved by performing real module-level validation measurements. There is also potential for refining the mesh settings. For now, an easy-to-use and stable setting has been used for productivity. For larger numbers of models, increasing the efficiency of the process, possibly through automation, could further improve quality. However, it makes use of several simplifications, which, in some cases, can be disadvantageous in larger, more complex geometries. For a cost-effective module design, it seems to make sense to opt for a close-coupled cell layout and to focus on optimizing heat dissipation through the module walls. It will minimize the size of the module and also avoid the need for additional cooling components, which would increase the system's complexity and could be a source of failure. The simple design thus also facilitates a wide range of applications.

The simulation approach presented in this paper can be used in various applications, including small and large battery systems. While systems with fewer cells are easier to test during and after assembly, thermal testing of larger systems is more complex (e.g., vehicles). Furthermore, in cases where the batteries are subjected to higher loads, possibly in trucks and trains, it further complicates the design of the battery storage system. Different vehicles should be arranged with different battery placements and insulation (packaging, boxing). Therefore, the same battery may heat differently in a second vehicle. Therefore, designing the cooling and heating of these systems is a challenging and complex task. In such cases, battery thermal simulation considerations can be particularly useful, as a well-fitted model can help in the design process. Heat transfer and conduction problems can be identified in such cases, and overheating or inadequate heating of the battery system can be avoided (extraction capacity can be drastically reduced in extreme cases). Furthermore, simulations can be used cost-effectively to investigate the effect of different cases (external temperature and load) on the system temperature.

Author Contributions

Conceptualization, S.K.S. and G.K.; methodology, S.K.S., G.K., M.S., J.L. and S.F.; software, S.K.S. and G.K.; validation, S.K.S., G.K., M.S., J.L. and S.F.; formal analysis, S.K.S., G.K.; investigation, S.K.S., G.K., M.S., J.L. and S.F.; resources, S.K.S. and S.F.; data curation, S.K.S. and G.K.; writing—original draft preparation, S.K.S., G.K., M.S., J.L. and S.F.; writing—review and editing, S.K.S., G.K., M.S., J.L. and S.F.; visualization, S.K.S. and G.K.; supervision, M.S., J.L. and S.F.; project administration, S.K.S. and S.F.; funding acquisition, S.K.S. and S.F. The manuscript was written through the contribution of all authors. All authors discussed the results, reviewed, and approved the final version of the manuscript.

Acknowledgments

This paper was supported by the ÚNKP-22-4-II-SZE-26 New National Excellence Program of the Ministry for Culture and Innovation from the source of the National Research, Development and Innovation Fund.



Conflict of Interest

The authors declared no potential conflicts of interest concerning the research, authorship, and publication of this article.

Funding

The authors received no financial support for the research, authorship, and publication of this article.

Data Availability Statements

The datasets generated and/or analyzed during the current study are available from the corresponding author on reasonable request.

Nomenclature

A	Wall Surface Mesh (Area (m ²))	R	Universal gas constant (8314 J/kmol K)
E	Total energy, activation energy (J)	S	Total entropy (J/K)
g	Gravitational acceleration (m/s ²); standard value = 9.80665 m/s ²	S _n	Volumetric Heat Source (w/m ³ K)
h	Species enthalpy, standard state enthalpy of formation (energy/mass)	T	Temperature (K, °C.)
h _j	Sensible enthalpy (energy/mass)	t	The Shell Region thickness (m)
J _j	Mass flux; diffusion flux (kg/m ² /s)	U	Free-stream velocity (m/s)
k	Thermal conductivity (W/m/K, Btu/ft/h/°F)	V	Overall velocity vector (m/s)
k	The selected Material conductivity (For Shell Region) (W/m/K)	V _b	Cell volume (m ³)
K _{eff}	Effective Thermal conductivity (W/m/K)	W	Direction Z in descartes coordinate system
M	Molecular weight (kg/kmol)	μ	Dynamic viscosity (Pa.s)
P	Pressure (Pa)	ρ	Density (kg/m ³)
P _{op}	Operating pressure (Pa)	ρ ₀	Operation Density (kg/m ³)
		τ	Stress tensor (Pa)

Abbreviations

CFD	Computational Fluid Dynamics
BTMS	Battery Thermal Management System
TMS	Thermal management systems
PCM	Phase Change Material
HP	Heat Pipe
CAE	Computer-aided engineering
PVC	Polyvinyl chloride
CC-CV	Constant current - Constant voltage

References

- [1] Shamshirband, M., Salehi, J., Gazijahani, F.S., Decentralized trading of plug-in electric vehicle aggregation agents for optimal energy management of smart renewable penetrated microgrids with the aim of CO₂ emission reduction, *Journal of Cleaner Production*, 200, 2018, 622-640.
- [2] Fischer, S., Kocsis Szürke, S., Detection Process of Energy Loss in Electric Railway Vehicles, *Facta Universitatis, Series: Mechanical Engineering*, 21(1), 2023, 81-99.
- [3] Fischer, S., Traction Energy Consumption of Electric Locomotives and Electric Multiple Units at Speed Restrictions, *Acta Technica Jaurinensis*, 8(3), 2015, 240-256.
- [4] Kocsis Szürke, S., Perness, N., Földesi, P., Kurhan, D., Sysyn, M., Fischer, S., A Risk Assessment Technique for Energy-Efficient Drones to Support Pilots and Ensure Safe Flying, *Infrastructures*, 8(4), 2023, 67.
- [5] Kocsis Szürke, S., Sütthö, G., Apagy, A., Lakatos, I., Fischer, S., Cell Fault Identification and Localization Procedure for Lithium-Ion Battery System of Electric Vehicles Based on Real Measurement Data, *Algorithms*, 15(12), 2022, 467.
- [6] Szalai, S., Kocsis Szürke, S., Harangozó, D., Fischer, S., Investigation of deformations of a lithium polymer cell using the Digital Image Correlation Method (DICM), *Reports in Mechanical Engineering*, 3(1), 2022, 116-134.
- [7] Kocsis Szürke, S., Dineva, A., Szalai, S., Lakatos, I., Determination of critical deformation regions of a lithium polymer battery by dic measurement and wowa filter, *Acta Polytechnica Hungarica*, 19(2), 2022, 113-134.
- [8] Yang, Y., Chen, S., Chen, T., Huang, L., State of Health Assessment of Lithium-ion Batteries Based on Deep Gaussian Process Regression Considering Heterogeneous Features, *Journal of Energy Storage*, 61, 2023, 106797.
- [9] Deng, D., Li-ion batteries: Basics, progress, and challenges, *Energy Science and Engineering*, 3(5), 2015, 385-418.
- [10] Grandjacques, M., Kuntz, P., Azais, P., Genies, S., Raccurt, O., Thermal Runaway Modelling of Li-Ion Cells at Various States of Ageing with a Semi-Empirical Model Based on a Kinetic Equation, *Batteries*, 7(4), 2021, 68.
- [11] Ling, J., Zhu, Z., *Battery Thermal Management Systems of Electric Vehicles*, M.Sc. Thesis, Department of Applied Mechanics, Division of Vehicle Engineering & Autonomous Systems, Road Vehicle Aerodynamics and Thermal Management, Chalmers University of Technology, Gothenburg, 2014.
- [12] Buidin, T.I.C., Mariasiu, F., Battery Thermal Management Systems, Current Status and Design Approach of Cooling Technologies, *Energies*, 4, 2021, 4879.
- [13] Olabi, A.G., Maghrabie, H.M., Adhari, O.H.K., Sayed, E.T., Yousef, B.A.A., Kamil, T.S.M., Abdelkareem, M.A., Battery thermal management systems: Recent progress and challenges, *International Journal of Thermofluids*, 15, 2022, 100171.
- [14] Kannan, C., Vignesh, R., Karthick C., Ashok, B., Critical review towards thermal management systems of lithium-ion batteries in electric vehicle with its electronic control unit and assessment tools, *Proceedings of the Institution of Mechanical Engineers, Part D: Journal of Automobile Engineering*, 235(7), 2021, 1783-1807.
- [15] Nelson, P., Dees, D., Amine, K., Henriksen, G., Modeling thermal management of lithium-ion PNGV batteries, *Journal of Power Sources*, 110(2), 2002, 349-356.
- [16] Pelegov, D.V., Chanaron, J.J., Electric Car Market Analysis Using Open Data: Sales, Volatility Assessment, and Forecasting, *Sustainability*, 15, 2023, 399.
- [17] Sharma, A., Zanotti, P., Musunur, L.P., Enabling the Electric Future of Mobility: Robotic Automation for Electric Vehicle Battery Assembly, *IEEE Access*, 7, 2019, 170961-170991.



- [18] Zhang, J., Li, X., He, F., He, J., Zhong, Z., Zhang, G., Experimental Investigation on Thermal Management of Electric Vehicle Battery Module with Paraffin/Expanded Graphite Composite Phase Change Material, *International Journal of Photoenergy*, 2017, 2017, 2929473.
- [19] Sääski, J., Riitahuhta, A., Multidomain simulations introduced in product development process, *International Conference on Engineering Design, ICED'07*, Paris, France, 227-228, 2007.
- [20] CFD Modeling of Battery with Transport Equations, <https://cfdflowengineering.com/cfd-modeling-of-battery-with-transport-equations> (Date of access: May 10, 2023)
- [21] Moukalled, F., Mangani, L., Darwish, M., *The finite volume method in computational fluid dynamics: an advanced introduction with OpenFOAM® and Matlab*, Springer, 2016.
- [22] Zou, Y., Zhao, X., Chen, Q., Comparison of STAR-CCM+ and ANSYS Fluent for Simulating Indoor Airflows, *Building Simulation*, 11(1), 2018, 165-174.
- [23] Welahettige, P., Vaagsaether, K., Comparison of OpenFOAM and ANSYS Fluent, Department of Process, Energy and Environmental Technology, *Proceedings of the 9th EUROSIM Congress on Modelling and Simulation, EUROSIM 2016, The 57th SIMS Conference on Simulation and Modelling SIMS 2016*, 142(148), 2016.
- [24] ANSYS, Inc. Ansys Fluent Theory Guide 2021 R2, July 2021.
- [25] ANSYS, Inc. ANSYS Fluent User's Guide, 15, November 2013.
- [26] Wang, Z., Ma, J., Zhang, L., Finite Element Thermal Model and Simulation for a Cylindrical Li-Ion Battery, *IEEE Access*, 5, 2017, 15372-15379.
- [27] Li, A., Yuen, A.C.Y., Wang, W., Chen, T.B.Y., Lai, C.S., Yang, W., Wu, W., Chan, Q.N., Kook, S., Yeoh, G.H., Integration of Computational Fluid Dynamics and Artificial Neural Network for Optimization Design of Battery Thermal Management System, *Batteries*, 8(7), 2022, 69.
- [28] Lloyd, R., Akrami, M.A., Critical Analysis of Helical and Linear Channel Liquid Cooling Designs for Lithium-Ion Battery Packs, *Batteries*, 8(11), 2022, 236.
- [29] Thermal Resistance – Thermal Resistivity, <https://www.nuclear-power.com/nuclear-engineering/heat-transfer/thermal-conduction/thermal-resistance-thermal-resistivity/2022>.

ORCID iD

Szabolcs Kocsis Szürke  <https://orcid.org/0000-0001-5639-8116>

Gábor Kovács  <https://orcid.org/0009-0007-8576-098X>

Mykola Sysyn  <https://orcid.org/0000-0001-6893-0018>

Jianxing Liu  <https://orcid.org/0000-0002-4779-7761>

Szabolcs Fischer  <https://orcid.org/0000-0001-7298-9960>



© 2023 Shahid Chamran University of Ahvaz, Ahvaz, Iran. This article is an open access article distributed under the terms and conditions of the Creative Commons Attribution-NonCommercial 4.0 International (CC BY-NC 4.0 license) (<http://creativecommons.org/licenses/by-nc/4.0/>).

How to cite this article: Kocsis Szürke S., Kovács G., Sysyn M., Liu J., Fischer S. Numerical Optimization of Battery Heat Management of Electric Vehicles, *J. Appl. Comput. Mech.*, 9(4), 2023, 1076–1092. <https://doi.org/10.22055/jacm.2023.43703.4119>

Publisher's Note Shahid Chamran University of Ahvaz remains neutral with regard to jurisdictional claims in published maps and institutional affiliations.

